

Signatures of spin blockade in the optical response of a charged quantum dot

E. G. Kavousanaki and Guido Burkard

Department of Physics, University of Konstanz, D-78464 Konstanz, Germany

(Dated: June 9, 2022)

We model spin blockade for optically excited electrons and holes in a charged semiconductor quantum dot. We study the case where the quantum dot is initially charged with a single electron and is then filled with an additional, optically excited electron-hole pair, thus forming a charged exciton (trion). To make contact with recent experiments, we model an optical pump-probe setup, in which the two lowest quantum dot levels (s and p shells) are photoexcited. Using the Lindblad master equation, we calculate the differential transmission spectrum as a function of the pump-probe time delay. Taking into account both spin conserving and spin-flip intraband relaxation processes, we find that the presence of the ground-state electron spin leads to an optical spin blockade at short delay times which is visible as a crossover between two exponential decays of the differential transmission. To make predictions for future experiments, we also study the dependence of the spin-blockade on an external magnetic field.

I. INTRODUCTION

One of the promising solid-state implementations for the realization of quantum computing that has been under intense study over the past years involves the use of a single electron spin confined to a charged quantum dot (QD)¹. The discrete QD energy structure allows for long spin lifetimes, e.g. exceeding one second in electrically defined GaAs QDs², in comparison with the bulk materials or semiconductor nanostructures of higher dimension. However, it has been shown that the inhomogeneous dephasing time T_2^* in GaAs QDs in the presence of an unpolarized ensemble of nuclear spins in the QD material is of the order of ~ 10 ns, while the intrinsic spin coherence time T_2 can reach values beyond $1 \mu\text{s}$ ³. The decoherence time is relevant for quantum information applications where it should exceed the elementary quantum gate operation time by a substantial factor. Electrical control of single spins has been realized in timescales of about 50 to 100 nanoseconds^{4,5}, while ultrafast optical pulses have been shown to allow ensemble spin manipulation in picosecond timescales^{6,7} and arbitrary coherent single-spin rotations⁸.

Spin blockade, more generally known as Pauli blockade, describes a situation where an electronic process is inhibited for certain spin configurations because the energetically accessible final states are forbidden by the Pauli exclusion principle (Fig. 1). In the electric transport between coupled quantum dots, spin blockade can prevent an electron to access an energetically favorable path due to spin conservation⁹ (Fig. 1a). Observations of the leakage current in the spin-blocking regime have allowed the study of spin decoherence mechanisms and in particular the role of nuclear spins^{10,11}.

In optical experiments, Pauli blocking effects, also known as phase space filling¹², are commonly observed in absorption spectra at high photoexcitation intensities or when ground state carriers are present. Spin blockade of the lower Zeeman branch in a singly charged QD in strong magnetic fields has been studied¹³, and in a recent pump-probe experiment¹⁴, signatures of optical spin

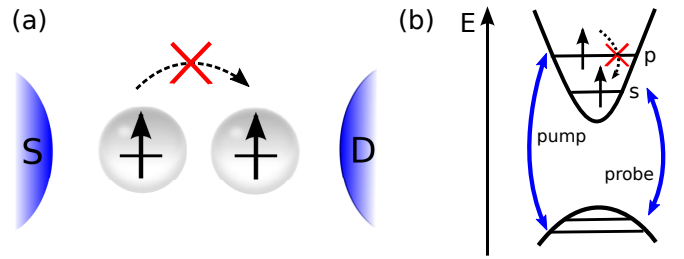


FIG. 1. (a) Spin blockade in charge transport through a double QD, connected to source (S) and drain (D) leads. A parallel spin configuration (spin triplet) can lead to a blocking of the current. (b) The optical analogy of spin blockade in the intraband relaxation between two QD levels s and p in a pump-probe set-up.

blockade have been observed in the transmission spectra of a charged QD. Lifting of spin blockade is typically more difficult to observe for optically excited carriers than for transport setups because electron-hole recombination processes can be much faster than the spin coherence and relaxation times.

In this paper, we describe an optical spin blockade effect in a charged quantum dot with two photoexcited energy levels that play the role of the two coupled QDs in transport. (Fig. 1b) We show the signature of interlevel (intraband) spin relaxation on the differential transmission signal in a pump-probe setup (Fig. 2) and draw the analogies between optical and transport experiments. For small QDs, the admixture mechanisms due to spin-orbit coupling play a smaller role¹⁵ and direct spin-phonon mechanisms need to be taken into account.

II. THEORETICAL MODEL

We study a quantum dot in a cubic semiconductor (e.g. GaAs) charged with a single electron. For self-assembled quantum dots, lateral dimensions are significantly larger than their height, and we thus we assume a circular quan-

tum dot in a parabolic confinement potential characterized by a frequency ω . In analogy with atoms, single particle eigenstates in QDs are typically labeled as s, p, d, \dots shell, which for our model correspond to $n = 0, 1, 2, \dots$ harmonic oscillator states, with $n = n_x + n_y$ the total quantum number. Including spin, single particle states in the conduction band are degenerate with respect to spin $J_z = \pm 1/2$ in the absence of a magnetic field (for circular QDs). In the valence band, heavy hole (total angular momentum $J_z = \pm 3/2$) and light hole ($J_z = \pm 1/2$) states are split due to confinement by an energy Δ_{lh} . Here, we will consider only heavy hole states, assuming that the heavy hole-light hole mixing near the band edges can be neglected.

The system is optically excited by a strong pump pulse that is resonant to the first excited QD state (p -shell), creating an electron-hole (e - h) pair with specific angular momentum depending on the pulse polarization. According to the optical selection rules, a right- (left-) circularly polarized σ_{\pm} pulse excites a $J_z = \mp 1/2$ electron and a $J_z = \pm 3/2$ hole, creating an excited trion state (Fig. 2). Depending on the spin polarization of the electrons, the (sp) trion state can be an electron singlet (total trion angular momentum $J_z = \pm 3/2$) or triplet ($J_z = \pm 5/2, \pm 3/2, \pm 1/2$)¹⁶. The singlet and triplet states are split by an energy Δ_{ee} due to electron-electron exchange interactions, which is typically of the order of a few meV. In our model, we assume that the pump pulse width is much broader than the singlet-triplet splitting Δ_{ee} and thus the latter can be ignored.

We focus on the interlevel relaxation of the photoexcited electron, i.e. relaxation from the (sp) trion state to the (ss) trion (see Fig. 2). Since the latter can only be an electron singlet, the relaxation rate depends strongly on the excited trion state. If it is a spin singlet, interlevel relaxation takes place through phonon emission on a timescale of a few tens of ns. On the other hand, if it is a spin triplet, a spin flip mechanism is required for the relaxation to take place. This will typically involve spin-orbit coupling in combination with phonon emission and take a much longer time as compared to the spin-conserving relaxation.

In our model, we use the Hamiltonian¹²

$$H = H_0 + H_L + H_C, \quad (1)$$

where

$$H_0 = \sum_{n\sigma} E_{n\sigma}^e \hat{e}_{n\sigma}^\dagger \hat{e}_{n\sigma} + \sum_{n\sigma} E_{n\sigma}^h \hat{h}_{n\sigma}^\dagger \hat{h}_{n\sigma}, \quad (2)$$

describes non-interacting electrons and holes and

$$H_L = - \sum_{n\sigma} dE(t) \hat{e}_{n\sigma}^\dagger \hat{h}_{n\bar{\sigma}}^\dagger - \sum_{n\sigma} d^* E^*(t) \hat{h}_{n\bar{\sigma}} \hat{e}_{n\sigma}, \quad (3)$$

is the coupling to the optical field, where $\hat{e}_{n\sigma}^\dagger$ ($\hat{h}_{n\sigma}^\dagger$), $\hat{e}_{n\sigma}$ ($\hat{h}_{n\sigma}$) are the creation and annihilation operators of an electron (hole) in the n -th quantum dot level ($n = s, p$)

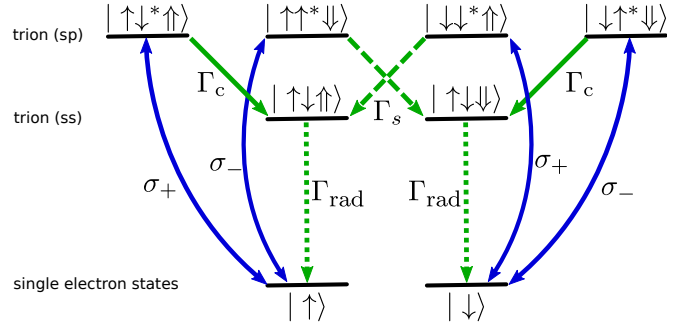


FIG. 2. Energy levels of a charged quantum dot under resonant photoexcitation with right- (left-) circularly (σ_{\pm}) polarized light of the first excited level (p shell), indicated by curved blue arrows. The electron (hole) spin in the lowest QD level (s shell) is denoted by \uparrow, \downarrow (\uparrow, \downarrow), while \uparrow^*, \downarrow^* denotes an electron spin in the excited QD level (p shell). Straight green arrows indicate relaxation processes with Γ_c the intraband spin-conserving relaxation rate, Γ_s the intraband spin-flipping rate, and Γ_{rad} the interband radiative recombination rate.

with spin $\sigma = \pm \frac{1}{2}$ ($\sigma = \pm \frac{3}{2}$), $E_{n\sigma}^e$ ($E_{n\sigma}^h$) the single-particle energies of the QD levels, d the interband dipole moment, and $E(t)$ the electric field. For a more compact notation, we use the notation $\bar{\sigma} = \uparrow, \downarrow$ when $\sigma = \downarrow, \uparrow$.

The last term in the Hamiltonian Eq. (1) describes Coulomb interactions,

$$H_C = \frac{1}{2} \sum_{nm\sigma\sigma'} V_{nm}^{ee} \hat{e}_{n\sigma}^\dagger \hat{e}_{m\sigma'}^\dagger \hat{e}_{m\sigma'} \hat{e}_{n\sigma} + \frac{1}{2} \sum_{nm\sigma\sigma'} V_{nm}^{hh} \hat{h}_{n\sigma}^\dagger \hat{h}_{m\sigma'}^\dagger \hat{h}_{m\sigma'} \hat{h}_{n\sigma} - \sum_{nm\sigma\sigma'} V_{nm}^{eh} \hat{e}_{n\sigma}^\dagger \hat{h}_{m\sigma'}^\dagger \hat{h}_{m\sigma'} \hat{e}_{n\sigma} \quad (4)$$

where only terms that conserve the number of particles in each QD level are included. This is a reasonable approximation for very small QDs in which interlevel spacing is much larger than Coulomb interaction. Such terms lead to density dependent energy shifts, as we will discuss in the next section.

Intraband relaxation of electrons from the p to the s shell is described with the Lindblad operators

$$L_{\sigma_1\sigma_2}^e = \hat{e}_{s\sigma_1}^\dagger \hat{e}_{p\sigma_2}. \quad (5)$$

Similarly, hole relaxation is described by the operator

$$L_{\sigma_1\sigma_2}^h = \hat{h}_{s\sigma_1}^\dagger \hat{h}_{p\sigma_2}, \quad (6)$$

The dynamics of the density matrix ρ describing the electronic state of the quantum dot is given by a master equation in the Lindblad form ($\hbar = 1$ throughout the paper),

$$\dot{\rho} = -i[H, \rho] + \sum_{\sigma_1\sigma_2r} \Gamma_{\sigma_1\sigma_2}^r [L_{\sigma_1\sigma_2}^r \rho L_{\sigma_1\sigma_2}^{r\dagger} - \frac{1}{2} L_{\sigma_1\sigma_2}^{r\dagger} L_{\sigma_1\sigma_2}^r \rho - \frac{1}{2} \rho L_{\sigma_1\sigma_2}^{r\dagger} L_{\sigma_1\sigma_2}^r], \quad (7)$$

where $r = e, h$ and

$$\Gamma_{\sigma_1\sigma_2}^e = \begin{cases} \Gamma_c & \text{if } \sigma_1 = \sigma_2 \\ \Gamma_s & \text{if } \sigma_1 \neq \sigma_2 \end{cases} \quad (8)$$

are phenomenological electron intraband spin-conserving and spin-flip relaxation rates. In a recent pump-probe experiment on a CdSe/ZnSe quantum dot¹⁴, the two relaxation rates have been estimated to be of the order of $\Gamma_s \sim 0.01 \text{ ps}^{-1}$ and $\Gamma_c \sim 0.1 \text{ ps}^{-1}$ respectively, corresponding to two well separated time scales.

Hole spin relaxation has been found to be much slower, of the order of $\tau_s^h = 1/\Gamma_{\sigma\bar{\sigma}}^h \sim 20 \text{ ns}$ ¹⁷ in both CdSe and InAs quantum dots and can be safely ignored here. We will only consider hole charge relaxation $\Gamma_h = \Gamma_{\sigma\sigma}^h$.

III. EQUATIONS OF MOTION

To compare with pump-probe experiments, we calculate the differential transmission signal $\Delta T/T$

$$\frac{\Delta T}{T}(\tau, \omega) = \frac{T_{\text{on}} - T_{\text{off}}}{T_{\text{off}}} \propto \text{Im}[P^{(3)}(\omega)], \quad (9)$$

where T_{on} (T_{off}) is the probe pulse transmission coefficient when the pump pulse is on (off), and $P^{(3)}$ is the induced polarization in frequency space in third order in the optical field.

The polarization is connected with the off-diagonal density matrix elements

$$P = d \sum_{n\sigma} P_{n\sigma}, \quad (10)$$

where

$$P_{n\sigma} = \langle \hat{P}_{n\sigma} \rangle = \langle \hat{h}_{n\bar{\sigma}} \hat{e}_{n\sigma} \rangle \equiv \text{Tr}[\hat{h}_{n\bar{\sigma}} \hat{e}_{n\sigma} \rho] \quad (11)$$

describes the interband excitation of an e - h pair in level n with spins σ and $\bar{\sigma}$ respectively. Here, we have introduced the average $\langle \dots \rangle \equiv \text{Tr}[\dots \rho]$. Using Eq. (7) with only two QD levels (s and p) per band and factorizing all four-operator expectation values within the Hartree-Fock approximation, the polarization dynamics is described by

$$\begin{aligned} i\dot{P}_{n\sigma} = & (E_{n\sigma}^e + E_{n\sigma}^h - V_{nn}^{eh} - i\gamma_P)P_{n\sigma} \\ & - dE(t)(1 - N_{n\sigma}^e - N_{n\sigma}^h) \\ & + P_{n\sigma} \sum'_{m\sigma'} U_{nm}(N_{m\sigma'}^e + N_{m\bar{\sigma}'}^h) \\ & - i\frac{P_{n\sigma}}{2} \sum_{\sigma'} \Gamma_{\sigma\sigma'}^e [\delta_{ns} N_{p\sigma'}^e + \delta_{np}(1 - N_{s\sigma'}^e)] \\ & - i\frac{P_{n\sigma}}{2} \Gamma_h [\delta_{ns} N_{p\bar{\sigma}}^h + \delta_{np}(1 - N_{s\bar{\sigma}}^h)] \end{aligned} \quad (12)$$

where

$$N_{n\sigma}^e = \langle \hat{e}_{n\sigma}^\dagger \hat{e}_{n\sigma} \rangle, \quad N_{n\sigma}^h = \langle \hat{h}_{n\sigma}^\dagger \hat{h}_{n\sigma} \rangle, \quad (13)$$

are electron and hole populations, and we have defined $U_{nm} = V_{nm}^{ee} - V_{nm}^{eh} = V_{nm}^{hh} - V_{nm}^{eh}$. The primed summation runs over all states $\{m\sigma'\} \neq \{n\sigma\}$, and polarization dephasing is described with a phenomenological dephasing rate γ_P .

The first three terms of Eq. (12) correspond to the semiconductor Bloch equations¹². The second term is the standard phase space filling term due to Pauli blocking, while the third term describes the renormalization of single particle energies due to Coulomb interactions. The last two terms describe a population-dependent dephasing of polarization due to electron and hole relaxation.

The dynamics of electron and hole populations is described by similar equations of motion,

$$\begin{aligned} i\dot{N}_{n\sigma}^r = & -i\gamma_N N_{n\sigma}^r - dE(t)P_{n\sigma}^* + d^* E^*(t)P_{n\sigma} \\ & + i\delta_{re} \sum_{\sigma_1\sigma_2} \Gamma_{\sigma_1\sigma_2}^e N_{p\sigma_1}^e (1 - N_{s\sigma_2}^e) (\delta_{ns} \delta_{\sigma_2\sigma} - \delta_{np} \delta_{\sigma_1\sigma}), \\ & + i\delta_{rh} \Gamma_h N_{p\sigma}^h (1 - N_{s\sigma}^h) (\delta_{ns} - \delta_{np}), \end{aligned} \quad (14)$$

with $r = e, h$ and γ_N the population relaxation rate. Again, the last two lines in Eq. (14) describe the effect of intraband $p \rightarrow s$ shell relaxation.

Since in pump-probe experiments the measurable quantities are at least third order in the optical field, the above equations may be expanded in terms of increasing order in $E(t)$, i.e. $P_{n\sigma} = P_{n\sigma}^{(1)} + P_{n\sigma}^{(3)} + O(E^5)$ and $N_{n\sigma}^r = N_{n\sigma}^{r(0)} + N_{n\sigma}^{r(2)} + O(E^4)$. Note that $N_{n\sigma}^{r(0)}$ is essentially the ground state population, which vanishes for undoped systems. In our case, assuming that the ground state electron lies in the lowest QD level, $N_{n\sigma}^{r(0)} = \nu_{n\sigma}^r = \delta_{re} \delta_{ns} \nu_{s\sigma}^e$ where $\nu_{s\sigma}^e$ is the s-shell filling factor.

In this manner we obtain a closed set of equations up to third order in the optical field, which are written explicitly in Appendix A. In the next section we will discuss their analytical and numerical solutions and calculate the differential transmission signal.

IV. RESULTS AND DISCUSSION

A. Analytical Solutions

The equations derived in the previous section can now be solved numerically for any exciting laser field $E(t)$. In the special case of ultrashort pump and probe pulses that can be described by delta functions, Eqs.(A1)-(A5) can be solved analytically. Even though in this case all QD levels can be excited (which is not the case in the experiment), analytical expressions provide useful insight for the dynamics and we will discuss them briefly in this section.

We assume an optical field that consists of two laser pulses propagating with time delay τ with respect to each other, i.e. it has the following form (at the QD):

$$E(t) = E_{\text{probe}}(t) + E_{\text{pump}}(t + \tau) \quad (15)$$

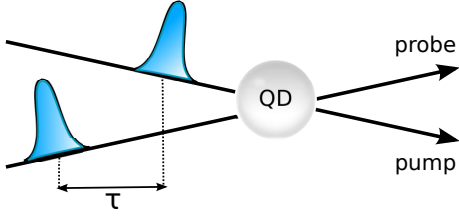


FIG. 3. Schematic representation of a typical pump-probe setup. The system is photoexcited by a strong pump pulse followed by a weaker probe pulse after time delay τ . The signal emitted in the direction of the probe pulse is measured as a function of τ .

where $E_i(t) = E_0^i \delta(t)$, $i = \text{pump, probe}$, and E_0^{probe} (E_0^{pump}) is the amplitude of the probe (pump) pulse that arrives at the system at time $t = 0$ ($t = -\tau$) (Fig. 3).

Using Eq. (15) in the equations of motion (for details see Appendix A), we obtain the interband polarization in first order in the optical field,

$$P_{n\sigma}^{(1)}(t) = id(1 - \nu_{n\sigma}^e) \left[E_0^{\text{probe}} e^{-iE_{n\sigma}t} e^{-\gamma_{n\sigma}t} \theta(t) + E_0^{\text{pump}} e^{-iE_{n\sigma}(t+\tau)} e^{-\gamma_{n\sigma}(t+\tau)} \theta(t+\tau) \right] \quad (16)$$

which consists of two parts due to the two pulses in the optical field.

For quantities that are second or third order in the optical field, we will only retain terms that are up to first order in the probe pulse, assuming that it is much weaker than the pump ($E_0^{\text{probe}} \ll E_0^{\text{pump}}$). In this case, the solution for the hole population, Eq. (A4), has the form

$$N_{n\sigma}^h(t) = |d|^2 (1 - \nu_{n\sigma}^e) E_0^{\text{pump}} \left\{ E_0^{\text{pump}} e^{-\gamma_n^{Nh}(t+\tau)} \theta(t+\tau) + E_0^{\text{probe}} e^{iE_{n\sigma}\tau} e^{-\gamma_{n\sigma}|\tau|} \times \left[\theta(\tau) e^{-\gamma_n^{Nh}t} \theta(t) + \theta(-\tau) e^{-\gamma_n^{Nh}(t+\tau)} \theta(t+\tau) \right] \right\} \quad (17)$$

which describes the creation of hole population in the n -th shell either from the pump pulse only, or from both the pump and probe pulses. Here we defined $\gamma_n^{Nh} = \gamma_N + (\delta_{np} - \delta_{ns})\Gamma_h$.

For the electronic populations we obtain similar expressions, but γ_N is replaced by a level-dependent relaxation rate $\gamma_{n\sigma}^{Ne} = \gamma_N + \delta_{np}(\nu_{n\sigma}^e \Gamma_c + \nu_{n\sigma}^e \Gamma_s)$ and there are additional terms of the form

$$\delta_{ns} \sum_{\sigma'} \left(e^{-\gamma_{s\sigma}^{Ne}t} - e^{-\gamma_{p\sigma'}^{Ne}t} \right)$$

that describe the rise of the s -shell electron population due to interlevel relaxation. These terms also appear in the solution for the third order terms $P_{n\sigma}^{(3)}$, and lead for a spin-dependent increase of the differential transmission signal as a function of the time delay. The exact expressions for $N_{n\sigma}^{e(2)}$ and $P_{n\sigma}^{(3)}$ are included in Appendix B.

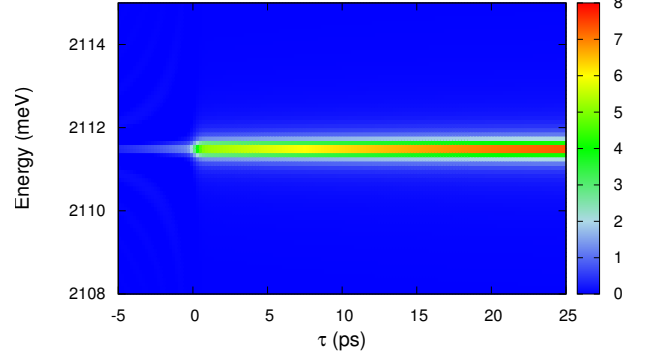


FIG. 4. Differential transmission signal $\Delta T/T$ (in arbitrary units) as a function of time delay τ and probe pulse energy $\hbar\omega$ for an unpolarized ground state electron, $\nu_{s\uparrow}^e = \nu_{s\downarrow}^e = 0.5$, and linearly polarized, Gaussian pulses with duration $T_{\text{pump}} = 700$ fs, $T_{\text{probe}} = 180$ fs. For this plot, we have used the parameters $E_s = 2110$ meV, $E_p = 2210$ meV, $\gamma_P = 5$ ps, $\Gamma_h = 0.1$ ps, $\Gamma_c = 15$ ps, $\Gamma_s = 170$ ps, $\gamma_N = 480$ ps, and $U_{nm} = 0$.

B. Zero magnetic field

In this section, we discuss the results from our numerical calculations of the differential transmission signal for Gaussian pulses similar to the experiment of Ref. 14. Fig. 4 shows the imaginary part of the nonlinear polarization $P^{(3)}(\omega)$ for the case of an unpolarized ground state electron as a function of the time delay τ between the pump and probe pulse and the probe pulse energy. There is a single peak at the s -shell trion energy E_s that increases with time delay for tens of picoseconds, in agreement of the signal is a signature of intraband relaxation from the p to the s shell, for which spin-conserving and spin-flipping mechanisms contribute, since the optical pulses are linearly polarized and the ground state electron unpolarized.

A more detailed description of the dynamics is shown in Fig. 5 which depicts snapshots of the signal for specific time delays. For $\tau = -2$ ps, for which the probe pulse precedes the pump, there is a small signal that arises from the interference between the two pulses and is characterized by oscillations with frequency $E_p - E_s$.

For $\tau = 2$ ps, when the probe pulse arrives right after the pump, the situation is different as the pump pulse has created an e - h pair in the p -shell. The hole relaxes almost immediately to the s shell in the valence band, and as the probe pulse arrives, it can either recombine with the ground state electron, or block the probe pulse absorption (bleaching), thus leading to an increase in the transmission.

For $\tau = 20$ ps, the electron has relaxed to the s -shell only if it is in the singlet configuration. Given that only two of the triplet states are bright, this leads to an addi-

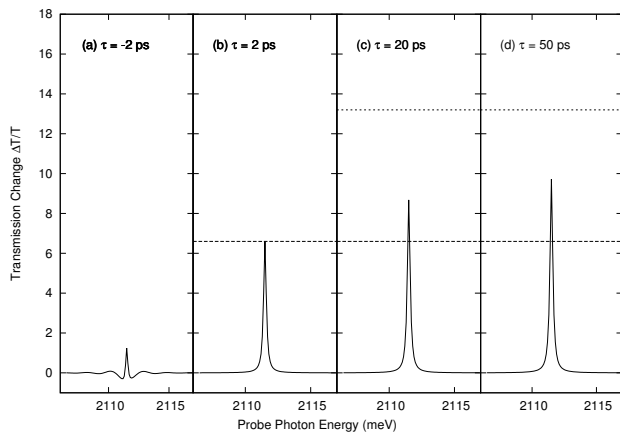


FIG. 5. Differential transmission signal as a function of probe pulse energy for different time delays τ . All parameters are as in Fig. 4. The dashed line marks the signal right after excitation by the pump pulse, that corresponds to bleaching due to hole interlevel relaxation. The dotted line marks the expected signal for full electronic relaxation.

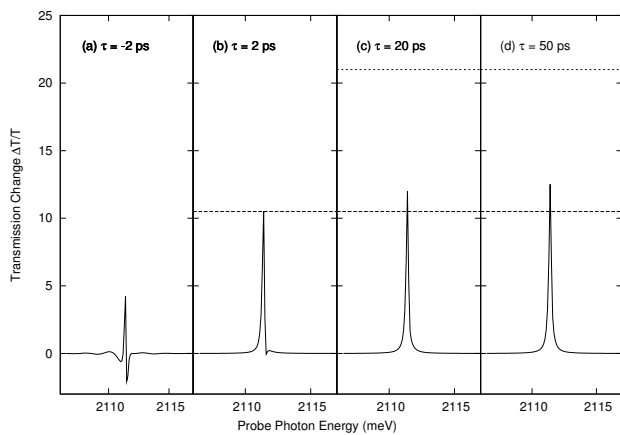


FIG. 6. Same as Fig. 5 but including Coulomb interactions ($U_{nm} = 0.1$ meV).

tional increase of the signal by a factor of ~ 1.3 in comparison to the signal at $\tau = 2$ ps, that remains constant for tens of picoseconds until spin flips can take place.

In the above results we have ignored the role of Coulomb interactions. Their contribution is shown in Fig. 6, which shows the differential transmission signal for the same parameters as in Fig. 5, but with the additional terms arising from Coulomb interactions. It is clear that their main effect is a shift of the fundamental trion resonance for very short timescales, but their role is diminished for larger time delays. This is in agreement with the results of Ref. 18, where the role of Coulomb correlations has been studied.

Fig. 7(a) shows the effect of electron spin relaxation on the differential transmission $\Delta T/T$ for a σ_+ pump pulse and a $\sigma = \downarrow$ ground state electron (in which case

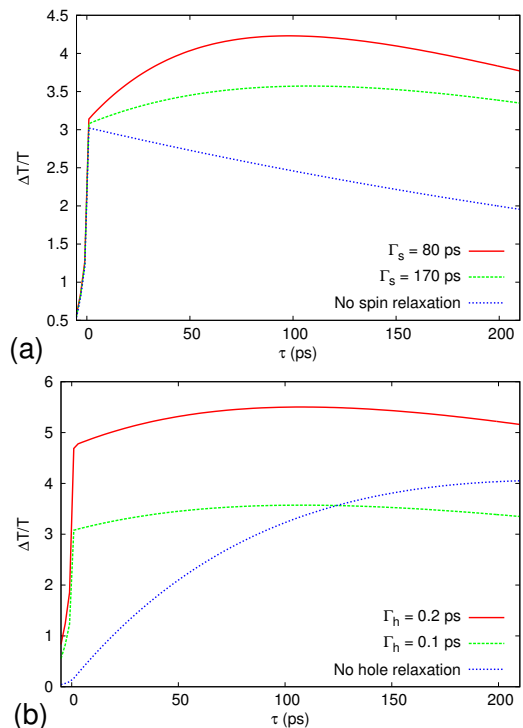


FIG. 7. Differential transmission signal as a function of time delay τ , (a) with and without the electron spin relaxation and (b) with and without hole relaxation for a $\sigma = \downarrow$ ground state electron and σ_+ polarized pump pulse. All other parameters are as in Fig. 4.

spin relaxation is necessary for interlevel relaxation). For small delay times τ , the slow spin-flip processes do not contribute and the signal exhibits a sharp increase due to hole relaxation. At larger time scales, the role of spin relaxation becomes evident by the slowly increase of the signal, the absolute maximum of which depends on the spin relaxation rate. As shown by the dotted line in Fig. 7(a), there is no increase of the signal in the absence of spin relaxation.

On the other hand, hole relaxation plays an important role at early timescales. This is shown in Fig. 7(b) where the differential transmission signal is plotted for different values of Γ_h . In the absence of hole relaxation, the signal increases slowly due to electron spin relaxation.

C. Finite magnetic field

In the presence of an external magnetic field, more spin relaxing mechanisms are allowed, thus enhancing the spin-flipping relaxation rate. It has been shown in Ref. 15 that spin relaxation in QDs is produced by a variety of mechanisms that can be separated in two groups: direct spin-phonon coupling, and admixture mechanisms due to spin-orbit coupling. In both cases though, the finite magnetic field leads to a $\sim B^2$ dependence of the

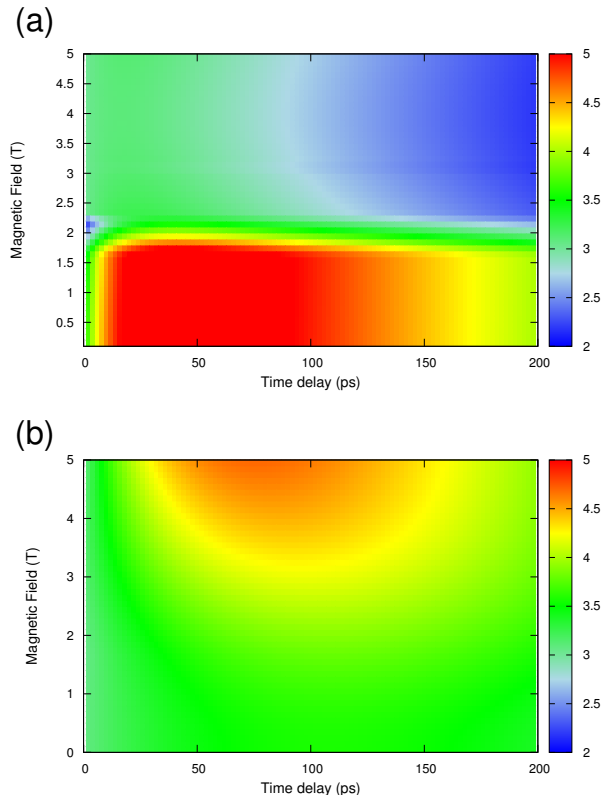


FIG. 8. Differential transmission $\Delta T/T$ as a function of pump-probe delay time τ and magnetic field B for a circularly polarized (a) σ_+ and (b) σ_- pump pulse. We assume the temperature is low enough for the ground state electron to be polarized. All other parameters are as in Fig. 4. In (a), the large spin-blockade signal for low magnetic fields is strongly suppressed at higher fields.

spin relaxation rate between different orbitals. For the quantum dots considered here^{14,19} and magnetic fields up to 5 T, Zeeman splitting is much smaller ($\sim \mu\text{eV}$)¹³ than the interlevel spacing (50 – 100 meV) and its role is insignificant. Thus, the admixture of different spin states plays a lesser role and the dominant spin flipping mechanism is the direct spin-phonon coupling.

In Fig. 8, the differential transmission signal at the s -shell resonance is shown as a function of time delay τ and magnetic field B for right and left circularly polarized pump pulses. Assuming that the temperature is low enough for the ground state electron to be fully polarized by the applied magnetic field, a σ_- pulse leads to a well defined spin blockade regime, as shown in Fig. 8(b). For low magnetic fields, the differential transmission signal is much smaller in comparison to Fig. 8(a) where spin conserving relaxation took place. However, due to the $\sim B^2$ enhancement of the spin flipping rate, at larger magnetic field spin blockade is suppressed. This in contrast with transport experiments where the application of an exter-

nal magnetic field suppresses the singlet-triplet mixing and thus enhances the spin blockade effect¹⁰.

V. CONCLUSIONS

We have developed a model describing the trion and population dynamics in a photoexcited quantum dot in a pump-probe setup. We have included the role of inter-subband relaxation including spin flipping and separated its role from the spin conserving mechanism. The long timescale of intraband spin relaxation leads to a signature in the differential transmission signal that is analogous to optical spin blockade. In the presence of an external magnetic field, the enhancement of spin-flipping relaxation rate leads to lifting of spin blockade at shorter time scales. This mechanism opens new possibilities for the study of spin decoherence processes in semiconductor quantum dots with optical probes.

ACKNOWLEDGMENTS

We acknowledge useful discussions with A. Leitenstorfer and funding from the Konstanz Center for Applied Photonics (CAP) and from BMBF under the program QuaHL-Rep.

Appendix A: Equations of motion

Here we write the set of equations, derived from Eqs. (12) and (14) expanded in increasing orders of the optical field. Keeping terms up to first order, Eq. (12) for the polarization becomes

$$i\dot{P}_{n\sigma}^{(1)} = (E_{n\sigma} - i\gamma_{n\sigma})P_{s\sigma}^{(1)} - dE(t)(1 - \nu_{n\sigma}^e), \quad (\text{A1})$$

where $E_{n\sigma} = E_{n\sigma}^e + E_{n\sigma}^h - V_{nn}^{eh} + U_{ns}$ is the trion energy and $\gamma_{n\sigma} = \gamma_P + \delta_{np}(\Gamma_c \nu_{s\bar{\sigma}}^e + \Gamma_s \nu_{s\sigma}^e + \Gamma_h)/2$ describes the trion relaxation rate, which for the p -shell is enhanced by the intraband spin-conserving and spin-flipping relaxation terms.

In second order in the optical field, the equations of motion for the electron and hole populations are

$$i\dot{N}_{s\sigma}^{e(2)} = -i\gamma_N N_{s\sigma}^{e(2)} - dE(t)P_{s\sigma}^{(1)*} + d^*E^*(t)P_{s\sigma}^{(1)} + i(1 - \nu_{s\sigma}^e) \left[\Gamma_c N_{p\sigma}^{e(2)} + \Gamma_s N_{p\bar{\sigma}}^{e(2)} \right], \quad (\text{A2})$$

$$i\dot{N}_{p\sigma}^{e(2)} = -i[\gamma_N + (1 - \nu_{s\sigma}^e)\Gamma_c + (1 - \nu_{s\bar{\sigma}}^e)\Gamma_s] N_{p\sigma}^{e(2)} - dE(t)P_{p\sigma}^{(1)*} + d^*E^*(t)P_{p\sigma}^{(1)}, \quad (\text{A3})$$

$$i\dot{N}_{n\sigma}^{h(2)} = -i(\gamma_N + (\delta_{np} - \delta_{ns})\Gamma_h) N_{n\sigma}^{h(2)} - dE(t)P_{n\sigma}^{(1)*} + d^*E^*(t)P_{n\sigma}^{(1)}. \quad (\text{A4})$$

Finally, for the polarization in third order, we obtain

$$\begin{aligned}
i\dot{P}_{n\sigma}^{(3)} &= (E_{n\sigma} - i\gamma_{n\sigma})P_{n\sigma}^{(3)} + dE(t) \left[N_{n\sigma}^{e(2)} + N_{n\sigma}^{h(2)} \right] \\
&+ P_{n\sigma}^{(1)} \sum_{m\sigma'} U_{nm} (N_{m\sigma'}^{e(2)} + N_{m\sigma'}^{h(2)}) \\
&+ i\frac{1}{2} P_{n\sigma}^{(1)} \Gamma_h (\delta_{np} - \delta_{ns}) N_{n\bar{\sigma}}^{h(2)} \\
&+ i\frac{1}{2} P_{n\sigma}^{(1)} \sum_{\sigma'} \Gamma_{\sigma\sigma'}^e \left(\delta_{np} N_{s\sigma'}^{e(2)} - \delta_{ns} N_{p\sigma'}^{e(2)} \right) \quad (\text{A5})
\end{aligned}$$

The last term in the above equation describes contributions from interlevel relaxation of electronic populations, which as discussed in section IV, leads to spin-dependent signatures in the differential transmission signal.

Appendix B: Analytical Solutions

The solution for the electronic populations has the form

$$\begin{aligned}
N_{n\sigma}^e(t) &= |d|^2 (E_0^{\text{pump}})^2 (1 - \nu_{n\sigma}^e) \theta(t + \tau) \left\{ e^{-\gamma_{n\sigma}^{Ne}(t+\tau)} \right. \\
&+ \delta_{ns} \sum_{\sigma'} a_{\sigma\sigma'} \left[e^{-\gamma_{s\sigma'}^{Ne}(t+\tau)} - e^{-\gamma_{p\sigma'}^{Ne}(t+\tau)} \right] \left. \right\} \\
&+ 2|d|^2 E_0^{\text{pump}} E_0^{\text{probe}} (1 - \nu_{n\sigma}^e) \left\{ \cos(E_{n\sigma}\tau) e^{-\gamma_{n\sigma}|\tau|} \right. \\
&\times \left[e^{-\gamma_{n\sigma}^{Ne}t} \theta(\tau) \theta(t) + e^{-\gamma_{n\sigma}^{Ne}(t+\tau)} \theta(-\tau) \theta(t + \tau) \right] \\
&+ \delta_{ns} \sum_{\sigma'} a_{\sigma\sigma'} \cos(E_{p\sigma'}\tau) e^{-\gamma_{p\sigma'}|\tau|} \\
&\left. \left[\theta(\tau) \theta(t) (e^{-\gamma_{s\sigma'}^{Ne}t} - e^{-\gamma_{p\sigma'}^{Ne}t}) \right. \right. \\
&\left. \left. + \theta(-\tau) \theta(t + \tau) (e^{-\gamma_{s\sigma'}^{Ne}(t+\tau)} - e^{-\gamma_{p\sigma'}^{Ne}(t+\tau)}) \right] \right\} \quad (\text{B1})
\end{aligned}$$

where $\gamma_{n\sigma}^{Ne} = \gamma_N + \delta_{np}(\nu_{n\bar{\sigma}}^e \Gamma_c + \nu_{n\sigma}^e \Gamma_s)$. and $a_{\sigma\sigma'} = \Gamma_{\text{sp}}^{\sigma\sigma'} / (\nu_{s\bar{\sigma}'}^e \Gamma_c + \nu_{s\sigma'}^e \Gamma_s)$. Comparing the above expression with the solution for the hole populations, Eq. (17), there are additional terms ($\propto \delta_{ns}$) that describe the creation of electronic population in the s -shell due to intraband relaxation.

The solution for the third order terms $P_{n\sigma}^{(3)}$, which contribute to the differential transmission signal, is given by (for $U_{nm} = 0$)

$$\begin{aligned}
P_{n\sigma}^{(3)}(\omega) &= (1 - \nu_{n\sigma}^e) \frac{dE_0^{\text{probe}} (E_0^{\text{pump}})^2}{\omega - E_{n\sigma} + i\gamma_{n\sigma}} \\
&\left[|d|^2 (e^{-\gamma_{n\sigma}^{Nh}\tau} + e^{-\gamma_{n\sigma}^{Ne}\tau}) \right. \\
&+ \delta_{ns} \sum_{\sigma'} a_{\sigma\sigma'} \left(e^{-\gamma_{s\sigma'}^{Ne}\tau} - e^{-\gamma_{p\sigma'}^{Ne}\tau} \right) \\
&+ \frac{1}{2} i (\delta_{ns} - \delta_{np}) \sum_{\sigma'} \frac{\Gamma_{\text{sp}}^{\sigma\sigma'} |d|^2}{\omega - E_{n\sigma} + i(\gamma_{n\sigma} + \gamma_{p\sigma'}^{Ne})} \\
&\times \left. \left(e^{-\gamma_{p\sigma'}^{Ne}\tau} + e^{-i(E_{n\sigma} - E_{p\sigma'})\tau} e^{-(\gamma_{n\sigma} + \gamma_{p\sigma'}^{Ne})\tau} \right) \right] \quad (\text{B2})
\end{aligned}$$

for $\tau > 0$ and

$$\begin{aligned}
P_{n\sigma}^{(3)}(\omega) &= (1 - \nu_{n\sigma}^e) \frac{dE_0^{\text{probe}} (E_0^{\text{pump}})^2}{\omega - E_{n\sigma} + i\gamma_{n\sigma}} \\
&\left[|d|^2 e^{-i(\omega - E_{n\sigma})\tau} e^{\gamma_{n\sigma}\tau} + \frac{1}{2} i (\delta_{ns} - \delta_{np}) \right. \\
&\times \sum_{\sigma'} \frac{\Gamma_{\text{sp}}^{\sigma\sigma'} |d|^2 e^{-i(\omega - E_{p\sigma'})\tau}}{\omega - E_{n\sigma} + i(\gamma_{n\sigma} + \gamma_{p\sigma'}^{Ne})} \left. (e^{\gamma_{n\sigma}\tau} + e^{\gamma_{p\sigma'}\tau}) \right] \quad (\text{B3})
\end{aligned}$$

for $\tau < 0$. Given that $\gamma_{n\sigma} \gg \gamma_{n\sigma}^{Ne}$, it is clear from the above solution that the differential transmission signal decays fast for $\tau < 0$, while for $\tau > 0$ it is dominated by the $\sim e^{-\gamma_{n\sigma}^{Ne}\tau}$ term at long timescales, leading to spin-dependent decay.

- ¹ D. Loss and D. P. DiVincenzo, Phys. Rev. A, **57**, 120 (1998).
- ² R. Hanson, L. P. Kouwenhoven, J. R. Petta, S. Tarucha, and L. M. K. Vandersypen, Rev. Mod. Phys., **79**, 1217 (2007).
- ³ J. R. Petta, A. C. Johnson, J. M. Taylor, E. A. Laird, A. Yacoby, M. D. Lukin, C. M. Marcus, M. P. Hanson, and A. C. Gossard, Science, **309**, 2180 (2005).
- ⁴ F. H. L. Koppens, C. Buizert, K. J. Tielrooij, I. T. Vink, K. C. Nowack, T. Meunier, L. P. Kouwenhoven, and L. M. K. Vandersypen, Nature, **442**, 766 (2006).
- ⁵ K. C. Nowack, F. H. L. Koppens, Y. V. Nazarov, and L. M. K. Vandersypen, Science, **318**, 1430 (2007).
- ⁶ A. Greilich, D. R. Yakovlev, A. Shabaev, A. L. Efros, I. A. Yugova, R. Oulton, V. Stavarache, D. Reuter, A. Wieck, and M. Bayer, Science, **313**, 341 (2006).
- ⁷ A. Greilich, A. Shabaev, D. R. Yakovlev, A. L. Efros, I. A. Yugova, D. Reuter, A. D. Wieck, and M. Bayer, Science,

317, 1896 (2007).

- ⁸ J. Berezovsky, M. H. Mikkelsen, N. G. Stoltz, L. A. Coldren, and D. D. Awschalom, Science, **320**, 349 (2008).
- ⁹ K. Ono, D. G. Austing, Y. Tokura, and S. Tarucha, Science, **297**, 1313 (2002).
- ¹⁰ F. H. L. Koppens, J. Folk, J. M. Elzerman, R. Hanson, L. H. W. van Beveren, I. T. Vink, H. P. Tranitz, W. Wegscheider, L. P. Kouwenhoven, and L. M. K. Vandersypen, Science, **309**, 1346 (2005).
- ¹¹ O. N. Jouravlev and Y. V. Nazarov, Phys. Rev. Lett., **96**, 176804 (2006).
- ¹² H. Haug and S. W. Koch, *Quantum Theory of the Optical and Electronic Properties of Semiconductors*, 5th ed. (World Scientific, 2009).
- ¹³ A. Hoge, M. Kroner, S. Seidl, K. Karrai, M. Atature, J. Dreiser, A. Imamoglu, R. J. Warburton, A. Badolato, B. D. Gerardot, and P. M. Petroff, Appl. Phys. Lett., **86**, 221905 (2005).

- ¹⁴ F. Sotier, T. Thomay, T. Hanke, J. Korger, S. Mahapatra, A. Frey, K. Brunner, R. Bratschitsch, and A. Leitenstorfer, *Nature Physics*, **5**, 352 (2009).
- ¹⁵ A. V. Khaetskii and Y. V. Nazarov, *Phys. Rev. B*, **61**, 12639 (2000).
- ¹⁶ A. S. Bracker, D. Gammon, and V. L. Korenev, *Semiconductor Science and Technology*, **23**, 114004 (2008).
- ¹⁷ T. Flissikowski, I. Akimov, A. Hundt, and F. Henneberger, *Phys. Rev. B*, **68**, 161309 (2003).
- ¹⁸ J. Huneke, I. D'Amico, P. Machnikowski, T. Thomay, R. Bratschitsch, A. Leitenstorfer, and T. Kuhn, *Phys. Rev. B*, **84** (2011).
- ¹⁹ S. Mahapatra, K. Brunner, and C. Bougerol, *Appl. Phys. Lett.*, **91**, 153110 (2007).